Journal of Interfaces, Thin films, and Low dimensional systems 4 (2) Winter and Spring (2021) 385-392

DFT study of silicon channel effects embedded between armchair graphene nanoribbons with different widths on mechanical and electronic properties

Scientific research paper

Mehdi Zarepour*

Microwave/mm-wave and Wireless Communication Research Lab, Electrical Engineering Department, Amirkabir University of Technology, Tehran, Iran

ARTICLE INFO

Article history:
Received 8 October 2021
Revised 16 November 2021
Accepted 16 November 2021
Available online 10 December 2021

Keywords:
Graphene nanoribbon
Silicon channel
Bandgap
DFT

ABSTRACT

Graphene Nano-Ribbons (GNR) are strong candidates for future materials in the electronics industry. In this paper, we extract the mechanical and electrical properties of AGNRs combination of different widths and deposition of silicon dimer to create Metal-insulator-semiconductor by the DFT method. Results demonstrate that by decreasing the mean width and strain of AGNR-AGNR composite and replacing the carbon dimer with silicon dimer, the bandgap of the system will reduce. The AGNR-Si-AGNR composite is a promising candidate for transistor application due to the small bandgap and high current flow allowance because of the high electron state near the Fermi's level electronic state involvement under the bias voltage.

1 Introduction

Electronic devices are everywhere in our lives since miniaturization using the Nanoscale components has allowed extremely powerful devices to be portable. Graphene's unique mechanical, electrical, and thermal properties have attracted attention for various applications such as electronic applications [1,2]. Some of these properties are incredibly strong, about 200 times stronger than steel, high thermal conductivity (5 KW/mK), high electron mobility at room temperature (2.5×10^4 cm^2/V.s), high surface to the volume ratio (2630 m^2/g), and high modulus of elasticity (1TPa) [3]. Indeed, graphene's current density is 10^6 times greater than copper's current, and its mobility is estimated to be 250 times that of silicon. In addition to all of this, its flexibility and other properties make it ideal for various applications, from solar cells, battery technology, piezoelectric, touch screens, gas sensors, biosensors, and many others [4, 5].

Graphene does not possess a bandgap by itself; therefore, it cannot be used in electronics, which requires large current on/off ratios. In the case of nanoribbons, they may have the bandgap due to the width differences. For specific graphene ribbons of a few nm in width, the theory predicts that the bandgap varies as a function of the ribbon width W [6, 7] with ΔE(W) ~ 1eV 0 nm/W. This means that the bandgap of ~ 100 meV is expected for a ribbon of 10 nm, or conversely, a ribbon of width ~ 1 nm would be required to get the bandgap of silicon (~ 1 eV). As quantum confinement only relies on the geometric structure of the ribbon, the bandgap can in principle be varied by design, contrary to the fixed bandgap of a semiconductor like silicon. Moreover, graphene high mobility and high current

*Corresponding author.
Email address: Mehdizare@aut.ac.ir
DOI: 10.22051/jitl.2022.38021.1063

carrying capabilities, has motivated us to combine graphene nanoribbons with silicon to achieve a semiconductor composition or Schottky contact.

Graphene not only exhibits excellent mechanical, thermal, optoelectronic, and electrical properties but can also be combined with several organic materials to produce high-performance organic field-effect transistors [8]. From the semiconductor technology point of view, there are two incredible properties which make graphene more special than the other semiconductors, 1) zero-overlap with very high electron transfer, 2) zero bandgap opening at the Dirac point where conduction and valence bands meet each other [9]. This characteristic of semiconductors is due to the current flow over the gap between the valence band and conduction band. This flow can emerge with light absorption, heat, or external electric field induction. If the flow is generated by the external electric field to switch “on” and “off”, then it is called field-effect transistors (FETs) [10, 11]. Consequently, the bandgap should emerge in graphene for use as a semiconductor. There are several methods that have developed to imply bandgap in graphene, such as exposure to a vertical electric field, vacancy in the crystalline structure, adding impurities, dopant, oxidation, alloys, and decreasing the width of the graphene sheets [12].

Graphene strips, which have a width of several nanometers, are known as graphene nano-ribbons (GNR) [13]. Many studies focus on the electrical properties of GNR, which have shown the effects of the edges open to the bandgap [3,5,14]. The edges of these structures are classified into two different categories of armchairs and zigzags [3]. The zigzag structures can be metallic, but armchair structures can exhibit metal or semiconducting properties, which in a semiconductor state, the energy gap changes with the ribbon width [15]. Therefore, electrical properties in nanotechnology applications are characterized by the shape of the edge and width of the nanoribbon [16]. Fabrication of GNR has been reviewed by Celis et al. [12], and it has revealed that the bandgap varies in different fabrication mechanisms.

Recently, band engineering and elastic metallic and semiconductor properties of strained armchair GNR (AGNR) were studied by Prabhakar et al. [1]. They showed that the strained GNR passivized with hydrogen molecules could have large out-of-plane deformations demonstrating the properties of relaxed shape graphene.

The metal-semiconductor junction of GNR was studied by Hong et al. [17]. Four types of this junction have been simulated to show that the junction conductance strongly depends on the atomistic features of the access geometry from the metallic GNR to the semiconducting GNR. Sevinçli et al. [18] demonstrated that periodically repeated junctions of AGNRs of different widths formed multiple quantum well structures and showed that periodically repeating heterojunctions made of armchair graphene nanoribbons of different widths can form stable superlattice structures. Another junction is the semiconductor-semiconductor heterostructure (SSH) AGNR junction. SSH’s energy gap can be tunable, and it is possible to bring a bright future for graphene electronic applications [19]. Graphene heterojunctions are used in transistors [20] and photodetectors [21].

In this research, three types of AGNR metal-semiconductor junctions included GNR6(+)-GNR5, GNR6-GNR5(+), and GNR-Silicon-GNR (GSG), are analyzed by using the Density Functional Theory (DFT) method as shown in Fig.1. Silicon atoms have larger core dimensions than carbon, electrons in the valence band can participate more freely in the conduction process than carbon atoms. Consequently, a gate or channel forms in the Si atoms ambience.

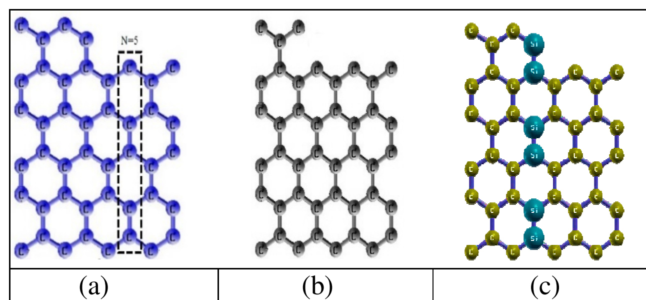

Figure 1. (a) Armchair GNR6(+)-GNNR5. (b) Armchair GNR6-GNNR5(+). (c) AGNR-silicon-AGNR-silicon (GSG) structure.

Their mechanical, electrical, and semiconductor properties have been studied by charge total energy, stress, strain, charge analysis, density of states (DOS) and band structure. A quantum espresso (QE) package has been used to study the structures. QE is an integrated suite of Open-source computer codes for electronic-structure calculations and materials

modelling. It is based on DFT, plane waves, and pseudopotentials [22].

2 Theoretical and computational method

DFT is a prevalent method for many-body systems by solving approximate versions of the Schrodinger equation [23, 24]. The accuracy of this method is noticeable [25]. This is not a single unit but usually comes as various parts, each intended to include some physical effects [6]. The electronic structure calculation employs the first principle method containing the self-consistent pseudopotential method [26-27] using the B3LYP[1]. Hybrid methods attempt to incorporate some of the more useful features from Abinitio or empirical methods (specifically Hartree-Fock methods) with some of the improvements of DFT mathematics while tending to be the most commonly used method for computational chemistry practitioners [23]. This method becomes one of the most popular semi-empirical hybrid functional methods [6,25].

To obtain the optimized atomic position and relax the atomic structure, an energy cutoff of 40 Ry is employed. A double plus polarization basis set is used for the localized basis orbitals to deal with the many atoms in a unit cell of the GNRs of various widths [28]. After relaxing the structures, self-consistent calculations are employed to extract the right plane waves, eigenvalues, eigenvectors, and Fermi's energy. Then, to cover all probable states, non-self-consistent calculations are carried with a 12*1*1 K-Point mesh in reciprocal space. In the next step, the K-Gamma-M-K route for electron motion vectors in reciprocal space is divided to 60 points to calculate energies and, consequently, the band structure of composites.

Furthermore, the DOS, charge analysis, and partial density of states are calculated. The same process has been done to extract GNR(6)-GNR(5) and GNR(6)-Si-GNR(5) properties and investigate the effects of the combinations, and silicon channel replaced by carbon dimer. The optimized distance between two lattices of 15 Å was employed to neglect the interaction between layers.

For AGNR with a width of N (N is the number of dimers) or ribbon width ($W = (N-3)\frac{\sqrt{3}}{2} + \sqrt{3}$), for $\frac{1}{W} \ll 1$, the bandgap's energy Δ_a is given by [7]:

$$\Delta_a \sim \begin{cases} 0, & N = 3m-1 \\ \frac{\pi}{W+\frac{\sqrt{3}}{2}}, & N = 3m \\ \frac{\pi}{W}, & N = 3m+1 \end{cases}, \tag{1}$$

where $m=1, 2, 3, 4, \ldots$. According to Eq. (1), the system is metallic when N=3m-1.

Here for m=2, N will be 5, 6, 7. For N=5 dimers, the bandgap is equal to 0 (as shown in Fig.2), and in the case of N = 6 from Equation (1), the bandgap is equal to 0.6 eV. To study the effect of the combination of N=5 and N=6 GNRs together without the intermediate channel, the configuration of two systems consisting of one more dimer from each GNRs with different widths like Fig. 1 has been considered. Following the previous study, the bandgap of the GNRs has an inverse relation with the GNRs width, and therefore, by increasing the GNR width, the bandgap will decrease [7].

Indeed, the bandgap has a direct [27] relation with strain. As strain increases, a small shift in minimum conduction and maximum valance band states will appear, and the current transmitted under bias voltage will increase with strain reduction. Therefore, strains are calculated for these structures from the young modulus and stress tensor.

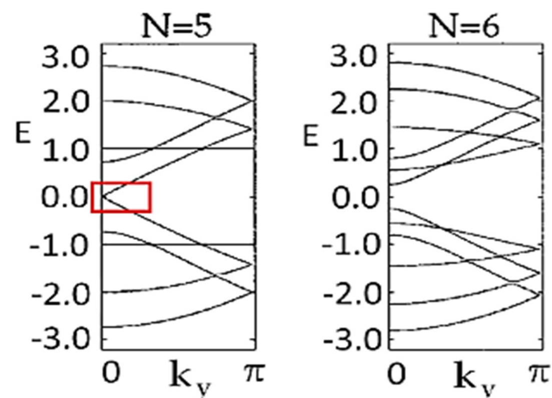

Figure 2. Band structure of N=5 dimers and N=6 dimers of AGNR [5, 28].

[1] Becke, 3-parameter, Lee-Yang-Parr

3 Results and discussion

After relaxing the structures, a bond length of 1.418 Å is obtained. The lowest energy is resulted in the GNR-Si-GNR configuration which indicates that this composite is more stable than other configurations. The flat structure remains for all of the composites where deflection or defect is found.

The DOS calculations are shown in Fig. 3 for all of the composites. The Fermi's level is shifted to 0. For the GNR6(+)-GNR5, most of the states are accommodated at the conduction band, but for the GNR6-GNR5(+) most of the states are located at the bottom of Fermi's level. In the case of GNR6-Si-GNR5, states are accumulated near the Fermi level. These results show that replacing the silicon channel modifies the semiconductor properties of the composite, and more current will appear under the bias voltage. Moreover, as shown in Table 1, Lowdin's charge analysis shows that by replacing the silicon channel with carbon dimer, charges from silicon atoms move toward the neighbor carbon dimers. This is another support for the DOS results, which is declared under the bias voltage, where more current will flow at the channel.

Normalized band structure diagrams are plotted in the K-Gamma-M-K path in the Brillouin Zone as shown in Fig. 4. The results of this section confirm the results discussed in the previous section. By decreasing the width of GNRs, the bandgap will decrease. For the GNR6(+)-GNR5 the bandgap value is equal to 0.3 eV which is very close to the theoretical predictions discussed in Eq. (1). For the GNR6-GNR5(+) configuration, the bandgap will decrease to 0.19 eV due to reduction in the mean width. However, the main result is the reduction of the bandgap energy due to the replacement of the carbon dimer by the silicon channel.

In case when the electrons of the valance band get closer to the conduction band in turn increases the current once the bias voltage employees due to the involvement of more states. Indeed, mechanical properties are calculated from the stress tensor and reported young modulus for GNRs before calculating the strain from $E = \sigma / \varepsilon$. The results are 0.0103, 0.0105, and 0.0078 for GNR6(+)-GNR5, GNR6-GNR5(+), and GNR6-Si-GNR5, respectively. These results are another witness to decreasing the bandgap by silicon dimer replacement. According to the claim of the previous section, by decreasing the strain of the system, the bandgap will decrease.

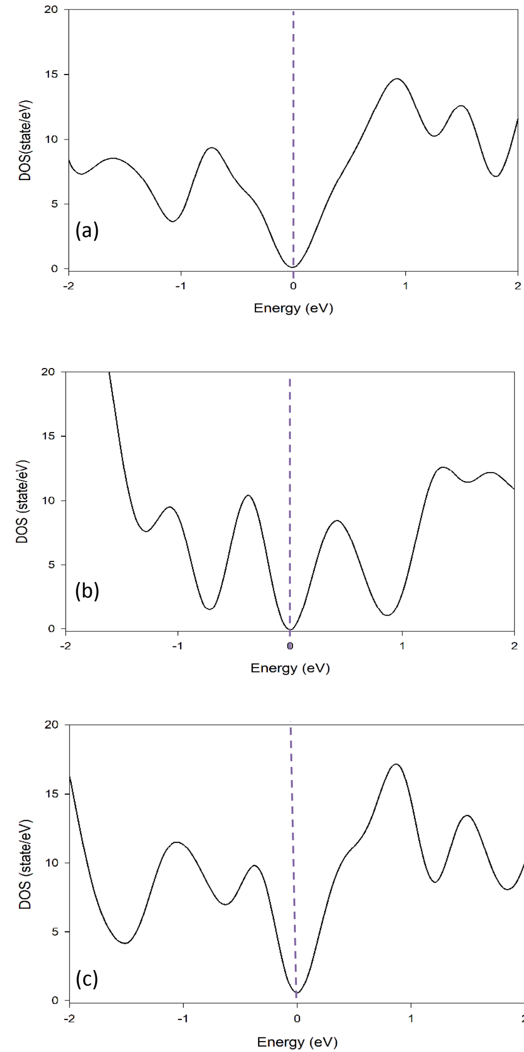

Figure 3. (a) DOS diagram of GNR6(+)-GNNR5. (b) Armchair GNR6-GNNR5(+). (c) AGNR-silicon-AGNR-silicon (GSG) structure.

I simulated the semiconductor AGNR with N=6 connects to metal AGNR with N=5, as shown in Fig. 1a. In the GNR-GNR (GG) structure, the energy band gap is modulated in real space where specific states are confined in certain segments [18] as shown in Fig. 2.

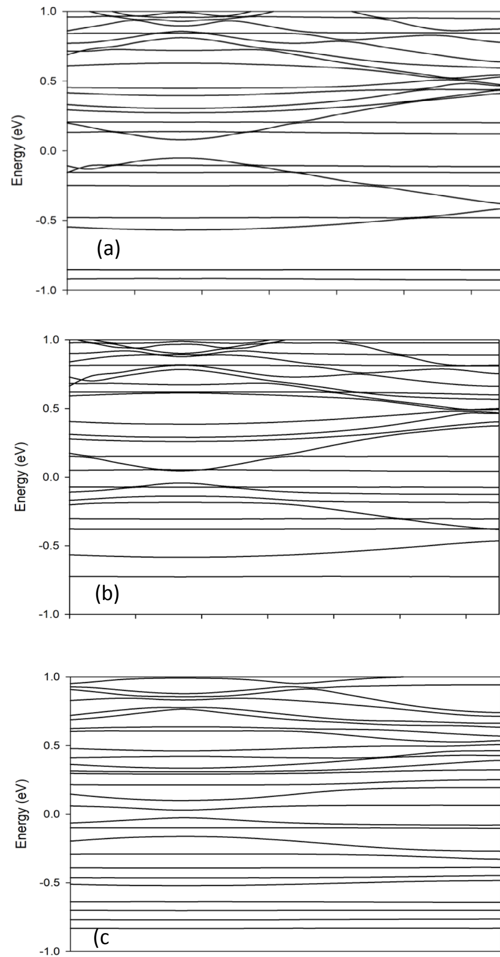

Figure 4. (a) Band structure diagram of GNR6(+)-GNNR5. (b) Armchair GNR6-GNNR5(+). (c) GNR-silicon-GNR-silicon (GSG) structure.

Table.1 Lowdin charges of atoms and orbitals near silicon channel

Left carbon dimer befor substitution of silicon channel	**Atom # 13: total charge = 3.9139, s = 0.9855, p = 2.9284,** **Atom # 14: total charge = 3.9348, s = 0.9282, p = 3.0066,** **Atom # 15: total charge = 3.9362, s = 0.9343, p = 3.0019,** **Atom # 16: total charge = 3.9244, s = 0.9336, p = 2.9908,** **Atom # 17: total charge = 3.9401, s = 0.9266, p = 3.0135,** **Atom # 18: total charge = 3.9783, s = 1.0648, p = 2.9136,**
Left carbon dimer after substitution of silicon channel	Atom # 13: total charge = 4.1718, s = 1.0299, p = 3.1419, Atom # 14: total charge = 4.1793, s = 1.0643, p = 3.1150, Atom # 15: total charge = 4.2036, s = 1.0257, p = 3.1778, Atom # 16: total charge = 4.1844, s = 1.0408, p = 3.1436, Atom # 17: total charge = 4.1953, s = 1.0285, p = 3.1668, Atom # 18: total charge = 4.2254, s = 1.0143, p = 3.2111,
Right carbon dimer befor substitution of silicon channel	Atom # 19: total charge = 3.8924, s = 1.0733, p = 2.8191, Atom # 22: total charge = 3.9295, s = 0.9238, p = 3.0057, Atom # 23: total charge = 3.9089, s = 0.9227, p = 2.9862, Atom # 26: total charge = 3.9047, s = 0.9401, p = 2.9646, Atom # 27: total charge = 3.9608, s = 0.9188, p = 3.0420,
Right carbon dimer after substitution of silicon channel	Atom # 19: total charge = 4.5762, s = 1.0889, p = 3.4873, Atom # 22: total charge = 4.1306, s = 1.0363, p = 3.0942, Atom # 23: total charge = 4.1925, s = 1.0258, p = 3.1667, Atom # 26: total charge = 4.1440, s = 1.0415, p = 3.1025, Atom # 27: total charge = 4.2363, s = 1.0081, p = 3.2282, Atom # 28: total charge = 3.8655, s = 0.9158, p = 2.9498,

Band structure calculations allow extracting partial density of states (PDOS), which represent the number of energy levels per unit energy that show the electronic coupling and orbital contributions. PDOS clearly explains the details of modifications in the energy band structure due to the bonding between Si and C atoms.

Moreover, to determine the bandgap opening and electronic characterization, by considering the shape of curves near the Fermi level, one can interpret the system. S, P_x, P_y, and P_z orbitals of silicon and carbon in the composite have been plotted to be compared together and to determine the overlap after the creation of bonds and whether the bonds are strong or not.

As shown in Fig. 5, the majority of S orbital states of carbon are placed between -22 and -15 eV, far from the Fermi level, and for the Silicon atoms, the majority of S orbital states are placed between -15 and -7.5 eV.

In the case of P_x orbitals of silicon and carbon atoms (as shown in Fig 6), for both orbitals, most states are placed between -10 and 5, and the main contribution lies in the construction of the bond.

For P_y orbitals of two atoms, as observed from Fig. 7, the states are distributed between -20 and 5 eV, but the strong peaks are at -5 to -10 eV. Common states are not as much as those for P_x orbitals. Due to the high overlap of these orbitals, they play a significant role in C-Si-Cbond formation.

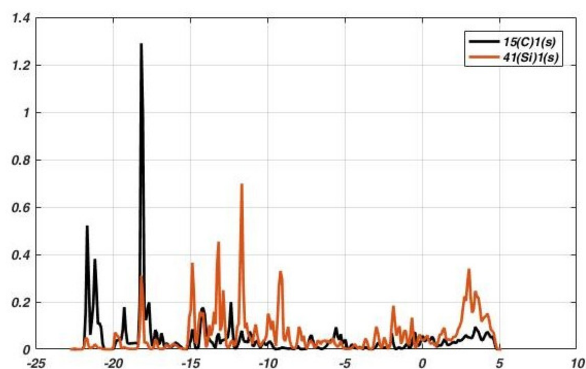

Figure 5. DOS versus Energy S orbit of Carbon and Silicon.

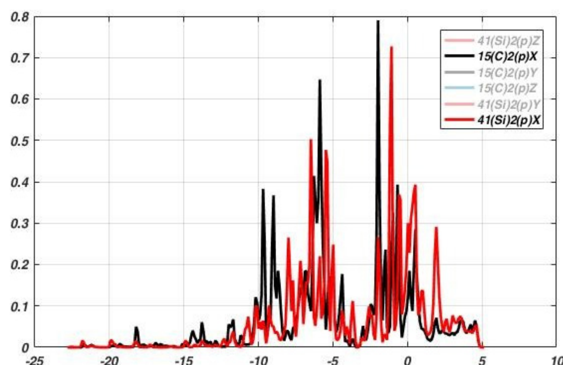

Figure 6. DOS versus Energy P_x orbit of Carbon and Silicon.

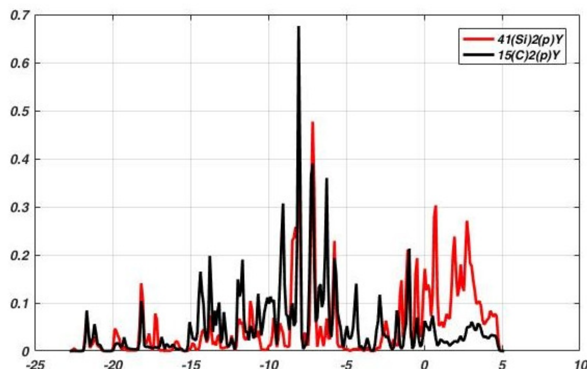

Figure 7. DOS versus Energy P_y orbit of Carbon and Silicon.

This comparison is also made for the pair of other orbits. Results demonstrate that these pairs have not significantly contributed to the bond. Among them, three pairs of above orbitals play an essential role in the formation of a strong bond due to the state overlaps.

4 Conclusions

In this study, it is found that the energy gap of the AGNR-Si-AGNR structure can be modulated in a wide range. Studies under DFT methods and quantum espresso (QE) packages show that the electronic properties of GNRs and their composites are functions of their widths and impurities. The composition of GNRs with different widths, can tune the bandgap and other properties, leading to design PN junctions. Moreover, by substitution of carbon dimer by the silicon dimer, this composite shows semiconductor properties, which can be used as the field effect transistors. It will show an increase in current flow under the external bias voltage due to the enhancement of electronic states near the Fermi energy.

Availability of data and materials

The datasets used and/or analyzed during the current study are available from the corresponding author on reasonable request.

Competing interests

The authors declare that they have no competing interests.

Funding

There is no funding.

Acknowledgment

I would like to thank Amirkabir University of Technology for supporting this research.

References

[1] S. Prabhakar, R. Melnik, "Band engineering and elastic properties of strained armchair graphene nanoribbons: semiconductor vs metallic characteristics." arXiv preprint arXiv:1901.00576, 2019.

[2] F. Schwierz, "Graphene transistors." Nature Nanotechnology, **5** (2010) 487.

[3] E. Kan, Z. Li, J. Yang, "Graphene nanoribbons: geometric, electronic, and magnetic Properties." Physics and Applications of Graphene-Theory, Sergey Mikhailov, IntechOpen (2011).

[4] J. Wang, M. Liang, Y. Fang, T. Qiu, J. Zhang, L. Zhi, "Rod-coating: towards large-area

fabrication of uniform reduced graphene oxide films for flexible touch screens." Advanced Materials, **24** (2012) 2874.

[5] M. Aliofkhazraei, N. Ali, W. I. Milne, C. S. Ozkan, S. Mitura, J. L. Gervasoni, Graphene Science Handbook: Nanostructure and Atomic Arrangement: CRC Press (2016).

[6] J. R. Reimers, "Computational methods for large systems: electronic structure approaches for biotechnology and nanotechnology." John Wiley & Sons (2011).

[7] K. Wakabayashi, K.-i. Sasaki, T. Nakanishi, T. Enoki, "Electronic states of graphene nanoribbons and analytical solutions." Science and Technology of Advanced Materials, **11** (2010) 054504.

[8] F. Hao, X. Chen, "First-principles study of lithium adsorption and diffusion on graphene: the effects of strain." Materials Research Express, **2** (2015) 105016.

[9] D. R. Cooper, B. D'Anjou, N. Ghattamaneni, B. Harack, M. Hilke, A. Horth, et al., "Experimental review of graphene. International Scholarly Research Notices." **2012** (2012) 501686.

[10] F. Schwierz, "Graphene transistors." Nature Nanotechnology, **5** (2010) 487.

[11] N. Lu, L. Wang, L. Li, M. Liu, "A review for compact model of graphene field-effect transistors," Chinese Physics B, **26** (2017). 036804.

[12] A. Celis, M. Nair, A. Taleb-Ibrahimi, E. Conrad, C. Berger, W. De Heer, et al., "Graphene nanoribbons: fabrication, properties and devices." Journal of Physics D: Applied Physics, **49** (2016) 143001.

[13] T. Fang, A. Konar, H. Xing, D. Jena, "Mobility in semiconducting graphene nanoribbons: Phonon, impurity, and edge roughness scattering." Physical Review B, **78** (2008) 205403.

[14] A. Naeemi. J. D. Meindl, "Conductance modeling for graphene nanoribbon (GNR) interconnects." IEEE electron device letters, **28** (2007) 428.

[15] P. Zhao, M. Choudhury, K. Mohanram, J. Guo, "Analytical theory of graphene nanoribbon transistors." Design and Test of Nano Devices, Circuits and Systems, 2008 IEEE International Workshop on, pp. 3-6, 2008

[16] S. Mehmet Gokhan, "The effects of vacancy location and concentration on the transport properties of armchair and zigzag graphene nanoribbons." Materials Research Express (2019).

[17] S. Hong, Y. Yoon, J. Guo, "Metal-semiconductor junction of graphene nanoribbons." Applied Physics Letters, **92** (2008) 083107.

[18] H. Sevinçli, M. Topsakal, S. Ciraci, "Superlattice structures of graphene-based armchair nanoribbons." Physical Review B, **78** (2008) 245402.

[19] B. Fan and S. Chang, "Confined state energies in AGNR semiconductor–semiconductor heterostructure." Physics Letters A, **381** (2017) 319.

[20] Y. Lv, W. Qin, C. Wang, L. Liao, X. Liu, "Recent Advances in Low-Dimensional Heterojunction-Based Tunnel Field Effect Transistors." Advanced Electronic Materials, **5** (2019) 1800569.

[21] M. Moradinasab, M. Pourfath, M. Fathipour, and H. Kosina, "Numerical study of graphene superlattice-based photodetectors." IEEE Transactions on Electron Devices, **62** (2015) 593.

[22] http://www.quantum-espresso.org/resources/tutorials

[23] F. Giustino, "Materials modelling using density functional theory: properties and predictions" Oxford University Press (2014).

[24] R. M. Martin, "Electronic structure: basic theory and practical methods." Cambridge university press (2004).

[25] A. Shokuhi Rad, M. Esfahanian, S. Maleki, G. Gharati, "Application of carbon nanostructures toward SO_2 and SO_3 adsorption: a comparison between pristine graphene and N-doped graphene by DFT calculations." Journal of Sulfur Chemistry, **37** (2016) 176.

[26] E. Rudberg, P. Sałek, Y. Luo, "Nonlocal exchange interaction removes half-metallicity in graphene nanoribbons." Nano letters, **7** (2007) 2211.

[27] G. Gui, J. Li, and J. Zhong, "Band structure engineering of graphene by strain: first-principles calculations." Physical Review B, **78** (2008) 075435.

[28] Y. W. Son, M. L. Cohen, S. G. Louie, "Energy gaps in graphene nanoribbons." Physical review letters, **97** (2006) 216803.

[29] N. Merino-Díez, A. Garcia-Lekue, E. Carbonell-Sanromà, J. Li, M. Corso, L. Colazzo, et al., "Width-dependent band gap in armchair graphene nanoribbons reveals Fermi level pinning on Au (111)." ACS nano, **11** (2017) 11661.